

Nonlinear optics with full three-dimensional illumination

Rojiar Penjweini,^{1,2,*} Markus Weber,^{1,2} Markus
Sondermann,^{1,2,†} Robert W. Boyd,³ and Gerd Leuchs^{1,2,3}

¹*Friedrich-Alexander-Universität Erlangen-Nürnberg (FAU),
Department of Physics, Staudtstr. 7/B2, 91058 Erlangen, Germany*

²*Max Planck Institute for the Science of Light, Staudtstr. 2, 91058 Erlangen, Germany*

³*Department of Physics, University of Ottawa,
25 Templeton Street, Ottawa, Ontario K1N 6N5, Canada*

(Dated: February 2, 2022)

We investigate the nonlinear optical process of third-harmonic generation in the thus far unexplored regime of focusing the pump light from a full solid angle, where the nonlinear process is dominantly driven by a standing dipole-wave. We elucidate the influence of the focal volume and the pump intensity on the number of frequency-tripled photons by varying the solid angle from which the pump light is focused, finding good agreement between the experiments and numerical calculations. As a consequence of focusing the pump light to volumes much smaller than a wavelength cubed the Gouy phase does not limit the yield of frequency-converted photons. This is in stark contrast to the paraxial regime. We believe that our findings are generic to many other nonlinear optical processes when the pump light is focused from a full solid angle.

I. INTRODUCTION

The first multi-photon process was described by Göppert-Mayer when calculating the spontaneous decay of the $2s$ state of the hydrogen atom [1]. But it took until the invention of the laser and the first investigation of second-harmonic generation by *Franken* and coworkers in 1961 [2] before the field of nonlinear optics took off. Since then most of the experiments have been performed in the paraxial regime with mildly focused Gaussian beams, cf. Fig. 1a. One can find only a few reports on experiments where the pump light driving the nonlinear process has been focused such that the paraxial approximation is not valid [3–7]. These investigations treated second-harmonic generation at an interface [3, 4] or measured the nonlinear optical response of nano particles [5–7]. In a wider sense, also multi-photon-excitation microscopy [8] and stimulated-emission depletion microscopy (STED) [9] can be considered as nonlinear optics under non-paraxial conditions when using microscope objectives with large enough numerical aperture (NA) as depicted in Fig. 1b. There is even one report on STED in a 4Pi-microscopy setup using two microscope objectives [10], which however is still far away from full 4π solid angle focusing. Investigations in *isotropic* nonlinear media under clearly non-paraxial conditions are lacking.

Here, we investigate the nonlinear response under close to full-solid-angle focusing, when the transmitted beam interferes with the incoming beam to form a 4π standing wave (cf. Fig. 1c). Such a wave is a superposition of a converging (inward moving) and a diverging (outward moving) dipole wave [11, 12]. In this standing wave with a spherical phase front the wave vector of the

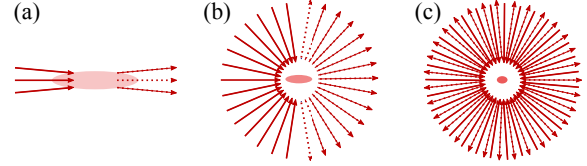


FIG. 1. Illustration of different focusing regimes: (a) paraxial regime using low NA. (b) non-paraxial regime of focusing with high NA. (c) focusing from a full solid angle. Solid/dotted arrows represent the propagation direction of a wave coming toward/going out of the focus. In non-paraxial regimes (b) and (c), the vector properties of the field are important. The rosé ellipse in the center indicates the size of the focal spot. Note that in (c) the spot is not spherical which is a result of the vector properties of the light, not shown in the diagrams.

pump naturally averages to zero, while the broad spread of wave vectors has implications on the phase matching of the nonlinear optical process, as we will discuss later. This is unlike the standing wave in a cavity, where the wave vectors are typically confined within a small cone. Furthermore, the focal volume within a standing dipole-wave is much smaller than a wavelength cubed [13, 14]. This is a new experimental regime in which no nonlinear optics experiments have been conducted so far. We perform such an experiment in studying a paradigmatic process, third-harmonic generation (THG) in an isotropic homogeneous medium (argon gas).

To focus the pump light from a full solid angle we use a parabolic mirror (PM) with a focal length much shorter than its depth. The PM is illuminated with a mode that after reflection off the PM surface resembles the radiation pattern of a linear electric dipole [15].

Under such conditions, several questions as posed below arise. In order to address these questions, we briefly recall some essential features of THG with Gaussian beams in the paraxial regime (see e.g. Ref. [16]): When the nonlinear medium

* rojiar.penjweini@mpl.mpg.de

† markus.sondermann@fau.de

is longer than twice the Rayleigh length of the Gaussian beam and the beam waist is located in the middle of the medium, the nonlinear polarization induced in the interaction region before the beam waist is 180 degree out of phase with the one generated in the diverging beam behind the beam waist due to the Gouy phase. Under conditions of nominal phase matching this results in destructive interference of the light fields generated in these two distinct half spaces. One can only compensate for the Gouy phase when choosing a nonlinear medium with a positive phase mismatch. Hence, in normally dispersive media such as noble gases driven far from resonance, where the phase mismatch is always negative, THG by four-wave mixing (FWM) ^{**} is not expected to occur (see e.g. section 2.10.3 in Ref. [16]). Thus, the generation of frequency-tripled photons can occur only as the result of higher-order processes, and accordingly the observed power dependence is not of third order (see e.g. Refs. [17–24]).

When focusing from a full solid angle with a dipole-like radiation pattern, the full width at half maximum of the spatial intensity distribution in the focus is on the order of the wavelength of the pump light or smaller. Consequently, the field amplitude of the pump light varies from practically zero to its maximum value within a wavelength and strictly violates the slowly-varying-amplitude approximation that is inherent to the paraxial approximation. Phase matching in the paraxial regime is equivalent to velocity matching such that the phase relation between pump, signal and idler is preserved. In the regime with light propagating in all directions this concept no longer makes sense. It will even turn out that over the relevant length scale of the focal pump field distribution the phase of the pump varies so weakly that it practically can be neglected.

Therefore, one can ask the general questions: “What determines the efficiency of the nonlinear coupling in this extreme case?”, “Which predictions of the paraxial approximation are still valid in the regime of extreme focusing” and “If one observes THG under this experimental condition, how will the third-harmonic signal scale with pump power and with the solid angle used for focusing?”

In this paper, we give answers to these questions. In Sec. II we describe our experimental apparatus and present the experimental results. As we will show, one indeed observes the generation of frequency-tripled photons when focusing from a large fraction of the full solid angle. Based on our observations, we identify six-wave mixing (SWM) as the underlying process, somewhat resembling other experiments in the paraxial regime [18, 23, 24]. Guided by this finding we compare our experimental observations to numerical simulations. In the last section, we discuss our

results and draw some further conclusions.

II. EXPERIMENT

A. Experimental setup

Figure 2 shows a simplified scheme of our experimental setup. A pulsed Nd:YAG laser is used as the light source for the fundamental beam. This laser has a wavelength of 1064 nm, a pulse duration of 2 ns, a repetition rate of 50 Hz and a pulse energy of up to 1 mJ. The beam power is adjusted by means of a half-wave-plate and a polarizing beam-splitter. The pump beam is transformed to a radially polarized doughnut beam by passing the fundamental Gaussian beam through a liquid-crystal polarization-converter (ARCoptix, RADPOL). Unwanted modes present in the beam leaving the polarization-converter are rejected by means of a spatial filter. Fig. 2b shows the intensity distribution and the orientation-angle of the local polarization vector of the resulting beam, both determined by a spatially resolved measurement of the Stokes parameters [25]. This mode has an overlap with the optimum mode for generating a linear dipole-wave in excess of 90%.

The pump beam is aligned to the PM by using two mirrors such that the beam propagates along the optical axis of the PM. The PM is made of aluminum and manufactured by single-point precision diamond-turning (Kugler GmbH, Germany). The focal length is $f = 2.1$ mm and the diameter of the exit PM’s pupil is 20 mm. In addition, the PM exhibits a bore hole of 1.5 mm diameter at its vertex. The PM is placed inside a vacuum chamber which is first evacuated to the order of 10^{-2} mbar and then filled with argon gas. The PM exhibits deviations from a perfect parabolic shape, introducing significant aberrations. The aberrations are characterized by interferometric measurements [26]. Based on the results of these measurements, a compensation mirror (CM) was manufactured which nominally imprints a wavefront modulation onto the incident beam that is conjugate to the one imprinted by the aberrations of the PM. The actual wavefront imprinted by the CM is also determined by interferometry. The CM serves as one of the alignment mirrors mentioned above (cf. Fig. 2a). In order to avoid changes to the imprinted wavefront occurring upon propagation, the electric field distribution emerging from the CM is imaged 1:1 onto the entrance aperture of the PM by means of a telescope.

We have assessed the impact of the PM’s aberrations and the degree of aberration compensation by the CM by simulating the focal intensity distribution for various cases exploiting all available interferometric data; see Fig. 2c. In comparison to an aberration-free mirror, the PM alone exhibits a Strehl ratio of only 19%, i.e., the maximum intensity in the focal region is about five times below that observed for diffraction-limited focusing.

^{**} By THG through FWM, we mean the process $\omega + \omega + \omega \rightarrow 3\omega$.

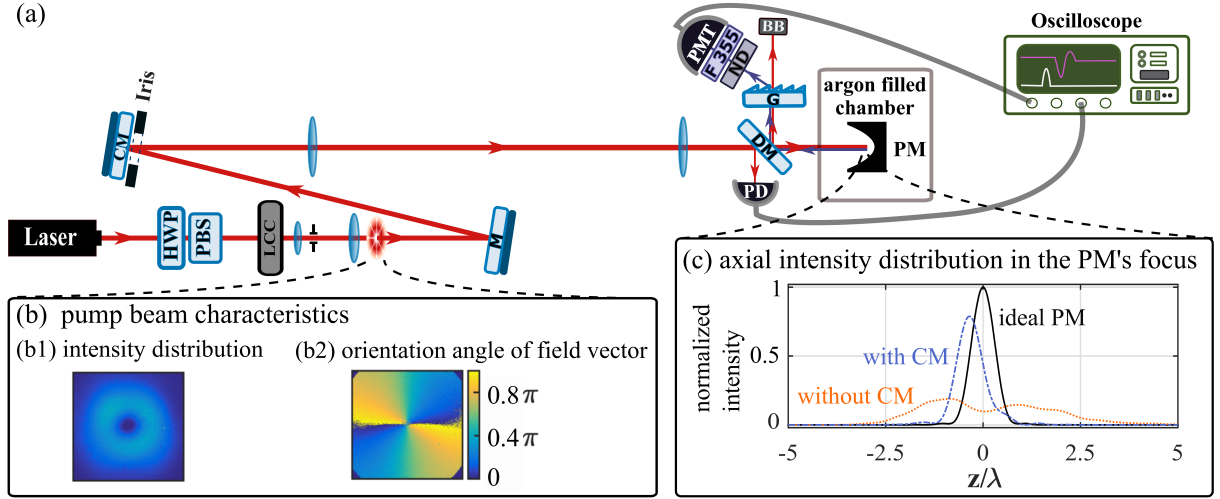


FIG. 2. (a) Scheme of the experimental setup. HWP: half-wave-plate, PBS: polarizing beam splitter, LCC: liquid-crystal polarization-converter, M: mirror, CM: compensation mirror, DM: dichroic mirror, PD: photodiode, PM: parabolic mirror, G: grating, BB: beam block, ND: neutral density filter, F 355: 355 nm laser-line filter, PMT: photomultiplier tube. (b) Intensity distribution (b1) and spatially resolved orientation angle ψ of the polarization vector (b2) of the pump beam. $\psi = 0$ is pointing parallel to the optical table and perpendicular to the optical axis of the PM. (c) Simulated axial intensity distribution in the focal region of an aberration-free PM (black, solid curve), the PM used in the experiments (orange, dotted curve), and for this PM when the aberrations are partially corrected by use of the CM (blue, dash-dotted curve).

However, the simulations predict that by using the CM the Strehl ratio can be improved to 79%. This imperfect compensation is due to the fact that the CM does not apply exactly the targeted phase distribution.

In the experiments presented below, we investigate the generation of TH photons using different solid angles for focusing. This variation is achieved by aperturing the pump beam with an iris of adjustable size. The iris is positioned close to the CM and is thus likewise imaged onto the PM aperture with the same telescope that is used for imaging the CM. By using the relation $\tan \vartheta/2 = r/2f$ [15] one can compute the effective half-opening angle ϑ for a given iris radius r . ϑ is then used for calculating the solid angle used for focusing.

Because a strongly focused, radially polarized doughnut beam produces an electric field distribution that closely resembles that of a linear dipole oscillating along the optical axis of the focusing device [27], here we define the solid angle as the one obtained when weighted with the angular intensity emission pattern of a linear dipole: $\Omega = 2\pi \int_{\vartheta_{min}}^{\vartheta_{max}} \sin^2 \vartheta \cdot \sin \vartheta d\vartheta$. Using this definition, Ω has an upper limit of $\frac{8\pi}{3}$ when $\vartheta_{min} = 0$ and $\vartheta_{max} = \pi$ [28]. The specific geometry of our PM corresponds to $\vartheta_{min} = 20^\circ$ and $\vartheta_{max} \simeq 134^\circ$. Therefore, the maximum weighted solid angle covered by our PM is $0.94 \times \frac{8\pi}{3}$.

Frequency-tripled photons generated in the focal region are collimated by the PM and afterwards reflected by a dichroic mirror (DM). The same DM directs a small fraction of the incident pump pulses onto a photodiode (PD). The PD signal serves as a trigger for detecting the frequency-tripled beam. To suppress any remaining pump light in the de-

tection path for the frequency-tripled photons, a grating (G) separates this light from the frequency-tripled beam. The pump beam is finally dumped at a beam block (BB). The frequency-tripled beam is detected by a photomultiplier tube (PMT, Hamamatsu R11540) after passing through a 355 nm laser line filter and neutral density (ND) filters. The PMT cannot distinguish between pulses with different photon numbers. It rather responds nonlinearly to pulses with more than one photon. Therefore, the ND filters are chosen such that they attenuate the frequency-tripled beam to an average photon number per pulse smaller than unity. In all experiments, the detected average photon-number per pulse is obtained from a series of about 2500-3000 laser pulses focused by the PM. Accounting for the attenuation factors of the used ND filters and other optical losses (in total 0.17%), we finally calculate the average number of frequency-tripled photons generated in the focal region of the PM.

B. Experimental results

At first, we check whether the generation of frequency-tripled photons under strongly non-paraxial conditions is observed at all. We monitor the number of photons detected at a wavelength of 355 nm while varying the diameter of the iris limiting the beam size from 7 mm to 20 mm. These diameters correspond to solid angles $36\% \leq \Omega/(8\pi/3) \leq 94\%$. The smallest solid angle investigated here corresponds to a half-opening angle of 80° or a NA of 0.98, respectively. Hence, all measurements are carried out under strongly non-paraxial conditions. For each iris diameter, the

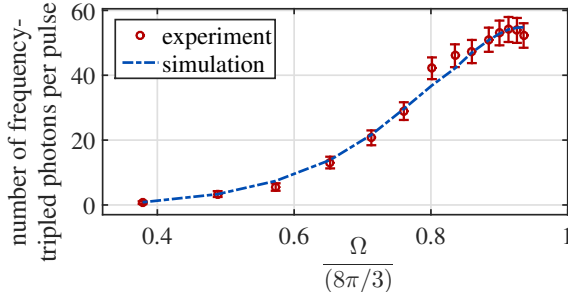


FIG. 3. Number of generated frequency-tripled photons versus the solid angle subtended by the pump beam. Red points show the experimental results for a pressure of 668 mbar and a fixed pump pulse energy of $114 \mu\text{J}$. The dash-dotted blue line shows the result of a simulation when using the nonlinear susceptibility $\chi^{(5)}$ as a fit parameter (cf. Sec. B for simulation details).

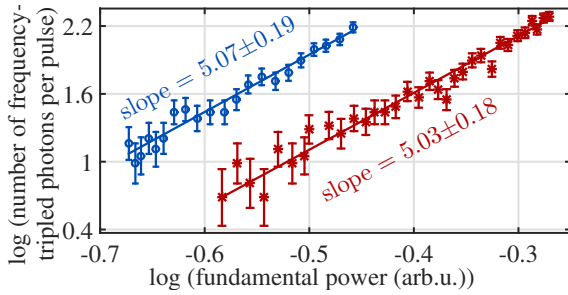


FIG. 4. Frequency-tripled photon generation vs. power of the fundamental beam at a pressure of 657 mbar for two different solid angles: 55% (red stars) and 94% (blue circles) of full solid angle. The data is presented in double logarithmic scale (symbols). The error bars are obtained from the Poisson statistics of the detected photons. The line denotes the result of fitting a linear function to the data.

laser power is adjusted such that the power transmitted through the iris is the same.

As is evident from Fig. 3, we indeed observe the generation of frequency-tripled photons. As one increases the solid angle used for focusing, one observes a higher yield of frequency-tripled photons. The number of frequency-tripled photons per pulse is affected by an interplay between the focal intensity and the focal volume as the main nonlinear interaction region, as discussed below. To investigate the generation of frequency-tripled photons in more detail and to unveil the mechanism of the frequency conversion, we measure the number of generated photons as a function of the peak power of the fundamental beam. Fig. 4 shows the results for two cases of focusing from 55% and from 94% of the full solid angle. A linear fit to the data in a double-logarithmic representation produces a line with a slope of approximately 5 in both cases. Thus, the number of the generated frequency-tripled photons scales with the fifth power of the optical power of the fundamental beam.

This result answers one of the questions posed above: Under strongly non-paraxial conditions, frequency-tripled photons are not generated by a

simple FWM process. In the paraxial regime, dependences of the frequency-tripled photon number on the pump power with orders ranging from 3.5 to 5 have been reported [17–24]. Possible explanations for this fifth-order dependence include a SWM process [18, 23, 24] and FWM with phase matching achieved by a Kerr effect [17, 20, 22]. However, our investigations exclude THG by FWM with phase matching enabled by the Kerr effect. As explained in detail in Appendix A, this conclusion results from the fact that for argon gas and the pump beam powers used in our experiment a positive phase mismatch cannot be achieved via the Kerr effect.

Therefore, as done elsewhere for several experiments in the paraxial regime [18, 23, 24], we attribute the generation of frequency-tripled photons in our experiments to SWM: The argon atoms absorb four photons at frequency ω and emit two photons, one of them with frequency ω and the other one with frequency 3ω . Unlike for THG with focused light, frequency-tripled generation through SWM is possible for both positive and negative phase mismatch [29]. In either case, in SWM one can compensate for the phase mismatch by suitable off-axis wave vectors (see also Ref. [23]). When focusing from large fractions of the solid angle, a broad spread of such wave vectors is readily provided.

Having identified the dependence of the THG on pump power, we now discuss the dependence of THG on solid angle in more detail: The intensity in the focus of the PM is proportional to the solid angle Ω [28]. Therefore, for a SWM process as found here one would expect the TH signal to scale with Ω^5 . However, the experimental data underlying Fig. 3 reveal a slightly weaker dependence (Ω^4). This dependence results from the fact that with increasing solid angle the focal volume decreases (see simulations in Fig. B.2 of App. B). The decrease of focal volume is weaker than the increase of the peak intensity in the focal region, resulting in the observed increase of TH photons when focusing from a larger solid angle.

Building upon these arguments, we simulate frequency-tripled photon generation, modeling the response of the medium with a fifth-order susceptibility. The detail of our theoretical simulation is explained in App. B.

In Fig. 3 we directly compare the simulation results to the experimental data. To within the experimental uncertainties we find a good qualitative agreement between simulation and experiment. By fitting the simulation results to the experiment we obtain $\chi^{(5)} = 1.53^{+0.21}_{-0.18} \times 10^{-48} (\text{m/V})^4/\text{bar}$ as the only fit parameter. This value is of the same order of magnitude as the value reported for the case of fifth harmonic generation in Ref. [30] and therefore appears to be reasonable. The main uncertainty of the fitting procedure is given by the accuracy of the pump power measurements, which is about 5%. Furthermore, in implementing our model numerically we made several approximations, cf. App. C,

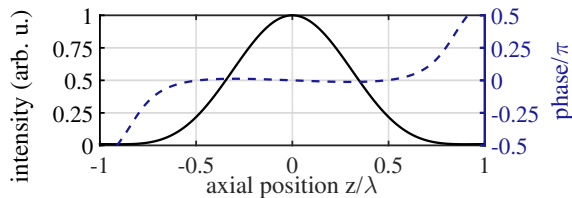


FIG. 5. Theoretical on-axis intensity (solid line) and phase distribution (dashed line) of the pump light on the optical axis of the PM when focusing with the complete PM covering 94% of the full solid angle without any aberrations.

which might influence the uncertainty of the value obtained for $\chi^{(5)}$. Nevertheless, we conclude that our model yields a good agreement with the experimental results.

III. DISCUSSION AND CONCLUSIONS

In the introduction of this paper we have raised several questions on potential differences between harmonic generation in the paraxial regime and when focusing the pump light from full solid angle.

Indeed, also in the latter case one observes the generation of frequency-tripled photons in an isotropic medium with normal dispersion. As in the paraxial regime, one does not observe a third-order dependence of the frequency-converted photons on pump power as expected for a FWM process. Rather, we have found a fifth-order dependence which hints at SWM as the underlying process.

What is the origin of the suppression of the FWM contribution to THG when focusing from a full solid angle? The tempting answer might be that the Gouy phase has the same detrimental effects as in the paraxial regime. And indeed, the standing spherical waves that are generated by focusing from a full solid angle exhibit the Gouy phase, i.e. a phase shift relative to a running spherical wave that emerges from the focus [31]. But being defined in such a way, the Gouy phase does not reflect the total phase at a certain position in the focal region. As our simulations reveal, the spatial variation of the phase of the pump field in the relevant focal region is not strong enough to result in a complete suppression of a FWM signal. As shown in Fig. 5, the intensity distribution of

the pump light decays more quickly towards zero than the phase of the pump field changes by $\pi/2$. This is clearly different from what is found for a focused Gaussian beam in the paraxial regime, for which a phase distribution as the one displayed in Fig. 5 can only be found when choosing an unphysical beam waist. The latter would correspond to a lateral width-at-half-maximum that is smaller than the minimal one obtainable in free space [14].

Another possible reason for the suppression of FWM is found when discussing wave vector diagrams (e.g. Refs. [16, 23]): For a FWM process in a normally dispersive medium, there is no combination of three wave vectors of the fundamental beam that results in a wave vector of the TH light. The wave vector mismatch is smallest for collinear wave vectors. In the experiment performed here, the strong focusing of the fundamental beam induces a large spread of the directions of the corresponding wave vectors. This large spread results in larger wave vector mismatches than in the paraxial regime. Hence the FWM process is suppressed even more strongly. Contrarily, for the SWM process focusing from full solid angle provides many possible combinations in which five wave vectors of the fundamental beam can be matched to a wave vector of the TH light. We thus conclude that SWM is the lowest-order process that can generate frequency-tripled photons in the case of very tight focusing.

Although we investigated the influence of full-solid-angle focusing on a specific nonlinear optical process, our findings – especially the ones about the role of the Gouy phase – are valid for all nonlinear optical processes, in particular to those of higher order. Furthermore, collecting the generated photons over a full solid angle minimizes losses and facilitates the investigation of the spatial properties of many phenomena in nonlinear optics.

ACKNOWLEDGMENTS

The authors thank K. Mantel for the characterization of the compensation mirror and M. Bader for discussions. GL acknowledges financial support from the European Research Council (ERC) via the Advanced Grant ‘PACART’. RWB acknowledges support through the Natural Sciences and Engineering Research Council of Canada and the Canada Research Chairs program.

[1] M. Göppert-Mayer, *Annalen der Physik* **401**, 273 (1931).
 [2] P. A. Franken, A. E. Hill, C. W. Peters, and G. Weinreich, *Phys. Rev. Lett.* **7**, 118 (1961).
 [3] E. Yew and C. Sheppard, *Optics Communications* **275**, 453 (2007).
 [4] D. P. Biss and T. G. Brown, *Opt. Lett.* **28**, 923 (2003).

[5] P. Reichenbach, A. Horneber, D. A. Gollmer, A. Hille, J. Mihaljevic, C. Schäfer, D. P. Kern, A. J. Meixner, D. Zhang, M. Fleischer, *et al.*, *Optics express* **22**, 15484 (2014).
 [6] A. Horneber, K. Braun, J. Rogalski, P. Leiderer, A. J. Meixner, and D. Zhang, *Physical Chemistry Chemical Physics* **17**, 21288 (2015).
 [7] X. Wang, X. Zhuang, F. Wackenhut, Y. Li, A. Pan, and A. J. Meixner, *Laser & Photonics*

- Reviews **10**, 835 (2016).
- [8] W. R. Zipfel, R. M. Williams, and W. W. Webb, *Nature Biotechnology* **21**, 1369 (2003).
 - [9] V. Westphal and S. W. Hell, *Phys. Rev. Lett.* **94**, 143903 (2005).
 - [10] M. Dyba and S. W. Hell, *Physical Review Letters* **88**, 163901 (2002).
 - [11] I. M. Basset, *Journal of Modern Optics* **33**, 279 (1986).
 - [12] C. Cohen-Tannoudji, J. Dupont-Roc, and G. Grynberg, *Photons and atoms* (J. Wiley and Sons, 1989).
 - [13] N. Bokor and N. Davidson, *Opt. Commun.* **281**, 5499 (2008).
 - [14] I. Gonoskov, A. Aiello, S. Heugel, and G. Leuchs, *Phys. Rev. A* **86**, 053836 (2012).
 - [15] N. Lindlein, R. Maiwald, H. Konermann, M. Sondermann, U. Peschel, and G. Leuchs, *Laser Physics* **17**, 927 (2007).
 - [16] R. W. Boyd, *Nonlinear optics, 3rd* (Academic press, 2008).
 - [17] R. A. Ganeev, M. Suzuki, M. Baba, H. Kuroda, and I. A. Kulagin, *Applied Optics* **45**, 748 (2006).
 - [18] R. Ganeev, S. R. Kamalov, M. Kodirov, M. Malikov, A. Rysnyansky, R. Tugushev, S. U. Umidullaev, and T. Usmanov, *Optics Communications* **184**, 305 (2000).
 - [19] G. Marcus, A. Zigler, and Z. Henis, *JOSA B* **16**, 792 (1999).
 - [20] M. S. Malcuit, R. W. Boyd, W. V. Davis, and K. Rzaewski, *Physical Review A* **41**, 3822 (1990).
 - [21] A. L’Huillier, L. Lompre, M. Ferray, X. Li, G. Mainfray, and C. Manus, *EPL (Europhysics Letters)* **5**, 601 (1988).
 - [22] R. Ganeev, V. Gorbushin, I. Kulagin, and T. Usmanov, *Applied Physics B: Lasers and Optics* **41**, 69 (1986).
 - [23] V. Vaičaitis, V. Jarutis, and D. Pentaris, *Physical Review Letters* **103**, 103901 (2009).
 - [24] V. Vaičaitis, V. Jarutis, K. Steponkevičius, and A. Stabinis, *Physical Review A* **87**, 063825 (2013).
 - [25] B. Schaefer, E. Collett, R. Smyth, D. Barrett, and B. Fraher, *American Journal of Physics* **75**, 163 (2007).
 - [26] G. Leuchs, K. Mantel, A. Berger, H. Konermann, M. Sondermann, U. Peschel, N. Lindlein, and J. Schwider, *Applied optics* **47**, 5570 (2008).
 - [27] S. Quabis, R. Dorn, M. Eberler, O. Glöckl, and G. Leuchs, *Opt. Commun.* **179**, 1 (2000).
 - [28] M. Sondermann, N. Lindlein, and G. Leuchs, *arXiv preprint arXiv:0811.2098* (2008).
 - [29] J. Kutzner and H. Zacharias, *Applied Physics B: Lasers and Optics* **66**, 571 (1998).
 - [30] X. F. Li, A. L’Huillier, M. Ferray, L. A. Lompré, and G. Mainfray, *Phys. Rev. A* **39**, 5751 (1989).
 - [31] T. Tyc, *Opt. Lett.* **37**, 924 (2012).
 - [32] M. N. Polyanskiy, “Refractive index database,” <https://refractiveindex.info> (2018), [Accessed on 2018-08-23].
 - [33] J. D. Jackson, *Classical Electrodynamics*, 3rd ed. (Wiley, New York, 1999).
 - [34] B. Richards and E. Wolf, in *Proceedings of the Royal Society of London A*, Vol. 253 (The Royal Society, 1959) pp. 358–379.
 - [35] L. Alber, M. Fischer, M. Bader, K. Mantel, M. Sondermann, and G. Leuchs, *Journal of the European Optical Society-Rapid Publications* **13**, 14 (2017), arXiv:1609.06884.

Appendix A: Influence of four-wave mixing and Kerr effect

It is well known that THG by FWM with light focused such that the beam waist lies in the middle of the interaction region is possible only if the phase mismatch, $\Delta k = 3k_1 - k_3$, is positive [16]. Here, k_1 is the wave number of the fundamental beam and k_3 is the wave number of the TH beam. In normal dispersive media (such as argon driven by 1064 nm light), with increasing frequency the refractive index increases and $\Delta k = \frac{6\pi}{\lambda_1}(n_1^{(0)} - n_3^{(0)})$ is negative, where λ_1 is the wavelength of the fundamental beam and $n_1^{(0)}$ and $n_3^{(0)}$ are the linear refractive indices for the fundamental beam and TH beam, respectively. Thus, THG by FWM is not possible in the normal dispersive media.

If THG is influenced by the Kerr effect, the phase mismatch will become a function of intensity and nonlinear refractive indices as

$$\Delta k_{\text{Kerr}} = \frac{6\pi}{\lambda_1}[(n_1^{(0)} - n_3^{(0)}) + (n_1^{(2)} - n_3^{(2)})I], \quad (\text{A1})$$

with $n_1^{(2)}$ and $n_3^{(2)}$ denoting the *nonlinear* refractive indices for fundamental and TH beam. I is the intensity of the fundamental beam. The nonlinear refractive index for a single intense fundamental beam with angular frequency ω is given by [16]

$$n_1^{(2)} = \frac{3}{4(n_1^{(0)})^2 \epsilon_0 c_0} \chi^{(3)}(\omega = \omega + \omega - \omega), \quad (\text{A2})$$

where ϵ_0 is the vacuum permittivity, c_0 is the speed of light in vacuum and $\chi^{(3)}$ is the third-order nonlinear susceptibility. The nonlinear refractive index for a weak frequency-tripled beam with angular frequency $\omega' = 3\omega$ in a medium influenced by an intense fundamental beam with angular frequency ω is [16]

$$n_3^{(2)} = \frac{3}{2(n_3^{(0)})^2 \epsilon_0 c_0} \chi^{(3)}(\omega' = \omega' + \omega - \omega). \quad (\text{A3})$$

Since the detuning of the pump as well as of the TH wave with respect to the lowest excited state of argon has the same sign, $\chi^{(3)}(\omega = \omega + \omega - \omega)$ and $\chi^{(3)}(\omega' = \omega' + \omega - \omega)$ have the same sign, too. Obviously, then the same holds true for $n_1^{(2)}$ and $n_3^{(2)}$.

From Eq. (A2) and Eq. (A3) we conclude that

$$n_1^{(2)} - n_3^{(2)} = \frac{3}{4\epsilon_0 c_0} \left(\frac{\chi^{(3)}(\omega = \omega + \omega - \omega)}{(n_1^{(0)})^2} - \frac{2\chi^{(3)}(\omega' = \omega' + \omega - \omega)}{(n_3^{(0)})^2} \right). \quad (\text{A4})$$

According to Eq. (A1), to get a positive Δk_{Kerr} and hence the possibility of THG for focused light, two conditions should be fulfilled. The first condition is

$$n_1^{(2)} - n_3^{(2)} > 0 \quad (\text{A5})$$

and the second condition reads

$$|(n_1^{(2)} - n_3^{(2)})I| > |(n_1^{(0)} - n_3^{(0)})|. \quad (\text{A6})$$

We cannot check the first condition quantitatively, because, to the best of our knowledge, the value of $\chi^{(3)}(\omega' = \omega' + \omega - \omega)$ for a strong beam at 1064 nm and a weak beam at 355 nm has not been reported. If $\chi^{(3)}(\omega = \omega + \omega - \omega)$ is sufficiently smaller than $2\chi^{(3)}(\omega' = \omega' + \omega - \omega)$ such that the first condition is not fulfilled, then THG by FWM will not be possible. However, assuming that $\chi^{(3)}(\omega = \omega + \omega - \omega)$ is greater than $2\chi^{(3)}(\omega' = \omega' + \omega - \omega)$ and knowing that $n_3^{(0)} > n_1^{(0)}$, the first condition given by Eq. A5 is fulfilled. With this assumption, we check the second condition, setting $n_1^{(2)} - n_3^{(2)} \cong n_1^{(2)}$ which is the case at which the intensity I needed to achieve the condition given by Eq. A6 is minimum.

Considering the linear refractive indices of argon at 1064 nm and 355 nm [32], we calculate $n_1^{(0)} - n_3^{(0)} \cong -2.6 \times 10^{-5}$. For the fundamental beam at 1064 nm, the third-order nonlinear susceptibility of argon gas is $\chi^{(3)} = 7.8 \times 10^{-27} \text{ (m}^2/\text{V}^2\text{)}/\text{bar}$ [30]. The maximum intensity which we reach just before the breakdown threshold in argon gas is about $3.5 \times 10^{13} \text{ W/cm}^2$. Our experimental measurements are always done below the breakdown threshold. Setting I to the intensity at the breakdown threshold and using Eq. (A2) to calculate the nonlinear refractive index, we conclude that $|(n_1^{(2)} - n_3^{(2)})I| \cong |n_1^{(2)}I| = 7.7 \times 10^{-7}$ which is more than an order of magnitude smaller than $|(n_1^{(0)} - n_3^{(0)})|$. The difference would be even more pronounced when $n_1^{(2)} \approx n_3^{(2)}$, since then $|(n_1^{(2)} - n_3^{(2)})I|$ would be even smaller. Therefore, even assuming most favorable conditions Eq. A6 cannot be fulfilled. Thus we conclude that the generation of frequency-tripled photons in our experiment is not the result of THG by FWM, even when phase matching is influenced by the Kerr effect.

Appendix B: Theoretical considerations

In what follows, we model the generation of frequency-tripled photons in the focus of a parabolic mirror.

The electric field of the incident focused beam induces a nonlinear polarization in the focal region of the PM. The contribution of the nonlinear polarization relevant for generating frequency-tripled photons is $\mathbf{P}_{3\omega}$. In section IIB we have argued that SWM is the responsible process for the generation of photons with frequency 3ω . Hence, we write

$$\begin{aligned} \mathbf{P}_{3\omega} &= \mathbf{P}^{(5)} \\ &= 5\epsilon_0 \chi^{(5)}(3\omega = \omega + \omega + \omega + \omega - \omega) \mathbf{E}^4(\mathbf{r}) \mathbf{E}^*(\mathbf{r}), \end{aligned} \quad (\text{B1})$$

where the factor 5 is the degeneracy factor, $\chi^{(5)}$ is the fifth-order nonlinear susceptibility and $\mathbf{E}(\mathbf{r})$ is the electric field of the focused fundamental beam. $\mathbf{r} = 0$ is the position of the geometrical focus of the PM.

Because $\mathbf{P}_{3\omega}$ is a dipole-moment density, the dipole moment oscillating at 3ω that is induced in a volume element V_i is given by

$$\mu_{3\omega,i} = \int_{V_i} \mathbf{P}_{3\omega} d^3\mathbf{r}. \quad (\text{B2})$$

In our simulations we associate V_i with the volume of a unit cell of the simulation grid. The light emitted by each dipole is collected by the parabolic mirror and propagates towards the detector. The detected signal is given by the interference of all these fields, with the amplitude of the field emerging from V_i being proportional to $\mu_{3\omega,i}$. We anticipate this interference process by introducing an effective dipole moment

$$M_{3\omega} = \sum_i \gamma_i \cdot \mu_{3\omega,i} \quad (\text{B3})$$

where the γ_i are real weighting factors that account for the projection onto a detection mode (see App. C for a discussion on the influence of the spatial separation of the dipole moments $\mu_{3\omega,i}$ onto the overall signal).

The total power that is radiated at frequency 3ω by the dipole moment $M_{3\omega}$ amounts to [33, Eq. 9.24]

$$W_{3\omega} = \frac{(3\omega)^4}{12\pi\epsilon_0 c_0^3} |M_{3\omega}|^2. \quad (\text{B4})$$

The medium is excited with pulses of Gaussian envelope of FWHM τ . Accounting for the observed 5th-order dependence of the THG photons on excitation power, the duration of the THG pulse is $\tau/\sqrt{5}$. Therefore, the number of frequency-tripled photons per pulse becomes

$$N_{3\omega} = \frac{W_{3\omega}\tau}{3\sqrt{5}\hbar\omega}, \quad (\text{B5})$$

where $3\hbar\omega$ is the energy of a frequency-tripled photon. Combining Eqs. (B2) to (B5) we arrive at

$$N_{3\omega} = \frac{225\epsilon_0\omega^3\tau\chi^{(5)^2}}{4\sqrt{5}\pi\hbar c_0^3} \left| \sum_i \gamma_i \int_{V_i} \mathbf{E}^4(\mathbf{r}) d^3\mathbf{r} \right|^2. \quad (\text{B6})$$

The complex electric field $\mathbf{E}(\mathbf{r})$ in the focal region of the PM is calculated by using the Debye integral method [34]. By integrating over complex fields we explicitly account for the spatial variation of the phase of $\mathbf{P}_{3\omega}$. In our calculations we take into account the measured aberrations of our PM, the measured phase-front induced by the CM as well as the field distribution of the radially polarized doughnut mode. All aberrations are modeled as relative phases of the electric field distribution incident onto the PM. The pulse energy and duration are the same as in the experiment underlying Fig. 3.

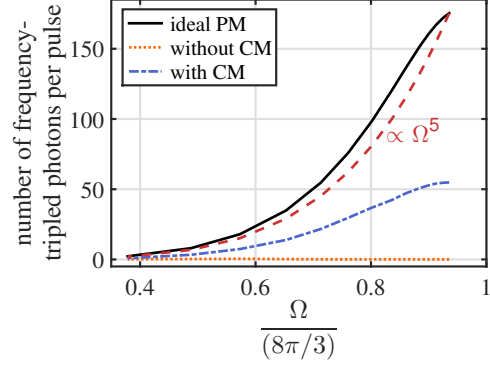


FIG. B.1. Simulated frequency-tripled photon number vs solid angle used for focusing. The dotted line is for the case of using our PM without correcting for its aberrations. The dash-dotted line is for the case of employing a CM in our setup, which compensates the aberrations of our PM up to a Strehl ratio of 79%. The solid line is for the case of an ideal PM without any aberrations. The dashed line denotes a curve $\propto \Omega^5$ for comparison. The absolute values of frequency tripled photons per pulse were obtained by fitting the case ‘with CM’ to the experimental data.

For the nonlinear susceptibility $\chi^{(5)}$ there is – to the best of our knowledge – no value reported in literature that was obtained in a comparable experimental setting, i.e. the generation of the TH of 1064 nm light by SWM. Ref. [30] reports $\chi^{(5)}$ for generating the fifth harmonic of 1064 nm light, whereas some $\chi^{(5)}$ values have been determined for SWM processes involving (deep) ultraviolet light, see Ref. [29] and references therein. Therefore, we here use $\chi^{(5)}$ as a fit parameter with which we quantitatively match the outcome of the simulations to the experimental results.

Fig. B.1 shows the result of simulating the generation of frequency-tripled photons as a function of the solid angle used for focusing. We consider three cases, as shown in Fig B.1.

In the first case, we model a PM without any aberrations, i.e. at the diffraction limit. The number of photons at frequency 3ω grows monotonically with increasing solid angle. This result can intuitively be understood from the fact that the focal intensity of the pump beam linearly with the solid angle Ω [28]. One would thus expect the conversion efficiency of an N -th order process to scale with solid angle as Ω^N . However, our simulation results do not show this Ω^5 dependence. We attribute this different result to the complicated spatial distribution of $\mathbf{E}(\mathbf{r})$ in the focal region: for increasing solid angle, the maximum intensity of the pump field in the focal region grows with Ω . However, the focal volume shrinks when increasing the solid angle (see simulations in Fig. B.2). Also the spatial distribution of the phase of $\mathbf{E}(\mathbf{r})$ changes upon varying Ω . All these effects result in the behavior observed in the simulation.

As a second case, we model the PM used in the experiments without any aberration compensation, the number of generated frequency-tripled

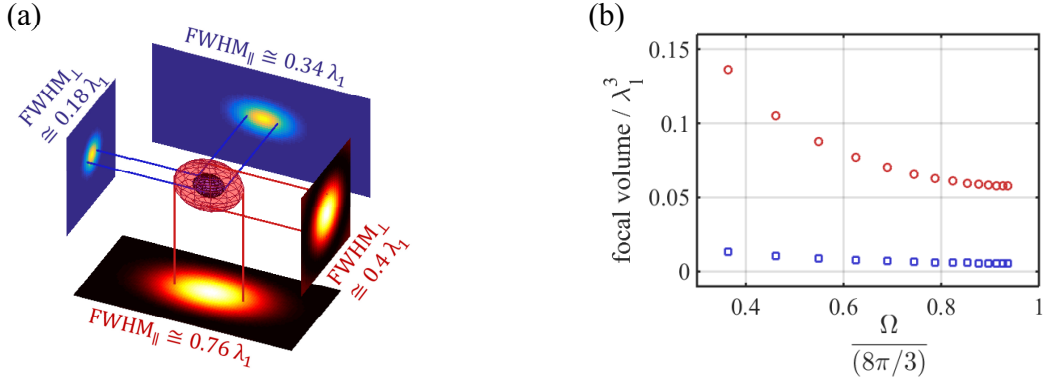


FIG. B.2. (a) Simulated focal volume of the fundamental beam focused by the PM (outer spheroid) and the effective volume in which the frequency-tripled beam is generated through SWM (inner spheroid). Aberrations of the PM are corrected for by using the CM. To obtain the respective volumes the FWHMs of the corresponding intensity distributions are determined. The effective volume of frequency-tripled generation is determined from the fifth power of the intensity distribution of the fundamental beam. The major axis of each spheroid equals the FWHM_{||} of the corresponding distribution along the axis of the PM and the minor axis is the FWHM_⊥ of the distribution in the focal plane perpendicular to the axis of the PM. (b) Focal volume vs. solid angle: The red circles correspond to the focal volume of the fundamental beam focused by PM. The blue squares correspond to the effective volume for frequency-tripled generation. All values are normalized to λ₁³ where λ₁ is the wavelength of the fundamental beam.

photons is very low at each investigated solid angle, cf. Fig. B.1. The maximum of ~ 0.5 photons per pulse occurs at a solid angle of $\Omega = 0.57 \cdot 8\pi/3$. That is, the steady increase of the photon number for increasing Ω is no longer observed. The latter observation can be explained by the spatial distribution of the aberrations over the surface of the PM. Similar effects are also observed for other parabolic mirrors [35]. Such aberrations appear to be typical for deep parabolic mirrors, and seem to represent the current state of the art.

Finally, as a third case we calculate the number of frequency-tripled photons for the case of compensating the aberrations of the PM with a CM, cf. Sec. II. This case is used to fit the simulations to the experimental results with $\chi^{(5)}$ as the only fit parameter. The simulation yields a steady increase of the photon number with increasing solid angle. Despite some saturation behavior at solid angle fractions beyond 90%, the results for the combination PM+CM shows *qualitative* similarities with the diffraction-limited case. However, the absolute photon numbers are considerably smaller than in the diffraction limited case. This latter observation is readily explained by the still non-optimum aberration compensation, which is expressed through a Strehl ratio of 79%. In the case of a nonlinear optical process as investigated here, the influence of a non-unit Strehl ratio should exponentiate to the order of the nonlinear process. For the largest solid angle used for focusing and for a fifth-order process, the simulation results approximately exhibit this behavior.

Appendix C: Collecting third-harmonic signals from spatially separated dipoles

In typical nonlinear optics experiments the light generated in a wave-mixing process is collected from an extended spatial region. This necessitates the account of the relative phases of the electric fields generated at different positions when calculating the total power that is generated in the nonlinear process. There are two contributions to the relative phases. One stems from the relative phase of the local pump field, which determines the phase of the nonlinear polarization. This contribution is directly included in our simulations, cf. Eq. B6. The second contribution is determined by the optical path-length difference (OPD) from the different source dipoles in the nonlinear medium to the point of detection. We now discuss how to account for this contribution in our particular scenario.

Whereas the OPD is readily defined in an experiment in which the detection occurs only under a small solid angle, the situation is more complicated when collecting light over the full solid angle. For two sources separated by a distance d the OPD to a point of observation lying on a circle with radius $\gg d$ is given by

$$\text{OPD} = d \cdot \cos \vartheta \quad (\text{C1})$$

with ϑ the angle to some reference direction. Thus, there is no unique OPD that is valid along all of the directions defined by the wave vectors of the dipolar emission of two separated sources. Moreover, the OPD is zero when averaging over ϑ .

However, when collecting light over the entire solid angle with a deep PM as in this work, the position of the light source determines the phase front of the mode that is reflected off the parabolic surface. These phase fronts can be expressed in terms

of misalignment functionals, which in general have to be calculated numerically by ray tracing [26]. For the experimental scenario treated here, we can make some simplifying assumptions that lead to analytic expressions.

First, the focused pump field is predominantly polarized parallel to the optical axis of the PM. Thus the nonlinear polarization and consequently all induced dipole moments oscillating at 3ω are oriented along this direction. Since the extent of the focus is on the order of a wavelength or even smaller, we assume that the intensity distribution of the emission of all these dipoles is the same as the one for a dipole located at the geometric focus of the mirror. After collimation by the PM and ignoring an overall amplitude factor this intensity distribution reads [15]

$$I(r) \propto \frac{(r/f)^2}{[(r/f)^2/4 + 1]^4} \quad (\text{C2})$$

with f the PM focal length and r the distance of a point in the aperture plane of the PM to the optical axis.

Second, the simulations of the focal intensity distribution of the pump light (cf. Sec. B) reveal that the electric field $\mathbf{E}(\mathbf{r})$ is effectively concentrated in a narrow region along the optical axis of the PM. Since we observe that the generation of frequency-tripled photons is proportional to the fifth order of the pump power, we examine the distribution of $|\mathbf{E}(\mathbf{r})|^{10}$. We find that the half-width at half-maximum of this distribution in lateral direction is about $0.1\lambda_1$ for using the full mirror. In the axial direction the width is slightly larger. For somewhat smaller solid angles, as was the case in

our measurements, the focal field distribution elongates along the optical axis while the lateral extent is practically constant. We therefore infer that the phase fronts of the TH light collected by the PM are mainly influenced by the axial position of the emitters and that phase front distortions due to lateral displacements can be neglected. Identifying ϑ in Eq. C1 with the emission angle of the dipole radiation pattern, the optical path-length difference of the emission from a dipole after collimation by the PM can be written as

$$\text{OPD}_i(r) = z_i \frac{1 - (r/2f)^2}{1 + (r/2f)^2} \quad , \quad (\text{C3})$$

where z_i is the axial displacement of the induced dipole $\mu_{3\omega,i}$ from the PM focus.

For calculating the interference of the fields emitted by all dipoles $\mu_{3\omega,i}$ in the focal region, we project each field distribution on a detection mode. We take the detection mode to be the field distribution that is emitted by the largest dipole moment. This dipole is located where the amplitude of the pump field is maximum, the corresponding axial coordinate is z_{\max} . Then, the overlap of the emission from dipole $\mu_{3\omega,i}$ with the detection mode reads

$$\gamma_i = \frac{\int I(r) \cdot \cos\left(\frac{6\pi}{\lambda_1}(z_i - z_{\max})\frac{1 - (r/2f)^2}{1 + (r/2f)^2}\right) r dr}{\int I(r) r dr} \quad , \quad (\text{C4})$$

with the integration performed over the entire aperture of the PM. This is the factor γ_i employed in the calculation of the number of frequency-tripled photons in Eq. B6 in the main part.